

Simulation of heat storages and associated heat budgets in the Pacific Ocean 1. El Niño-Southern Oscillation timescale

Guillermo Auad, Arthur J. Miller, and Warren B. White

Climate Research Division, Scripps Institution of Oceanography, University of California, San Diego, La Jolla

Abstract.

We use a primitive equation isopycnal model of the Pacific Ocean to simulate and diagnose the anomalous heat balance on El Niño-Southern Oscillation, ENSO, timescales associated with heat storage changes observed in the expendable bathythermograph (XBT) data set. We focus on the analysis of the total (diabatic plus adiabatic) and diabatic anomalous heat balances in six areas of the tropical and subtropical North Pacific Ocean in the upper 400 m. The diabatic (i.e., from the model conservation temperature equation) and adiabatic (i.e., from the model mass conservation equation) anomalous heat balances add up to the total anomalous heat balance. We computed the adiabatic/diabatic ratios to infer the relative importance of both contributions in different areas and found that they are smaller than 2.0 in only two regions (western equatorial and central North Pacific). The larger ratios (>2) were found along the corridor where adiabatic anomalies propagate westward in the form of Rossby waves and at the eastern equatorial Pacific. For those areas where the adiabatic/diabatic ratio is higher than about 2 the total anomalous heat balance is dominantly between the temporal change of heat and the three-dimensional divergence of the heat flux. At the central North Pacific area the total anomalous heat balance is between the temporal changes in anomalous heat, the surface heat flux and the vertical advection of heat. Different ENSO events are not always controlled by the same physical processes in the different areas. In many cases these differences are associated with the relative importance of adiabatic to diabatic processes. For instance, the western equatorial Pacific is controlled in general by diabatic processes, while the eastern equatorial Pacific is dominated by adiabatic physics most of the time.

1. Introduction

Upper ocean heat content (or storage) is a measure of the ocean's potential heat transfer to the overlying atmosphere and is thus an important climate variable. Although sea surface temperature (SST) directly interacts with the atmosphere through surface heat fluxes, variations in the temperature of the underlying fluid can eventually become manifest in SST through advection and mixing. However, the balance of physical processes that control the large-scale behavior of upper ocean heat content are still uncertain, in both a climatological and anomalous sense in most regions of the ocean. These physical processes include horizontal and vertical heat advection, ocean-atmosphere heat transfers and turbulent diffusion.

The classic picture of the upper ocean heat balance was developed by *Gill and Niiler* [1973] who showed that the large-scale balance is controlled by surface heat fluxes that drive the climatological seasonal changes in heat storage. This view was observationally substantiated by *Yan et al.* [1995], who showed that heat storage rate matches the net surface heat flux very well for 5° by 5° averages, though less well for 2° by 2° averages.

In regions with strong currents, the Gill-Niiler balance is likely to fail. Using hydrographic data, *Bryden et al.* [1991] estimate the meridional oceanic heat transported by oceanic velocity through 24°N . However, they point out the amount of heat transported by the North Pacific Ocean (NPO) is controversial given the wide range of values (and methods) reported by different authors. For instance, at subtropical latitudes in the NPO, Bryden et al. tabulate various estimates of heat transport that range between $1.14 \times 10^{15} \text{ W}$ northward and $1.17 \times 10^{15} \text{ W}$ southward.

Anomalous states of the midlatitude upper ocean heat content are even more uncertain. Studies of the

processes driving midlatitude SST anomalies [Cayan, 1992] would suggest that surface heat flux anomalies are likely to predominantly control upper ocean heat content. However, variability of the thermocline below the mixed-layer associated with large-scale ocean waves [e.g., Jacobs *et al.*, 1994; Miller *et al.*, 1997], atmospheric wind stress forcing [e.g., Liu, 1993; Miller *et al.*, 1998], coupled modes of variability [e.g., Latif and Barnett, 1994; Robertson, 1996] or other processes could significantly influence the integrated heat content.

The tropical heat budget has been studied in detail by many authors [e.g., Philander, 1990]. Most of the anomalous tropical ocean heat budget studies executed so far have used numerical models. Barnett *et al.* [1991] use a primitive equation numerical model applied to the tropics and find that advection dominates the oceanic SST heat balance, meridional advection being the most important in all regions except right on the equator. This term was largely dominated by Ekman dynamics. Miller *et al.* [1993] extended the Barnett *et al.* [1991] study to include two other Ocean General Circulation Models (OGCMs) and found that the anomalous SST heat budgets were different for each of the three GCMs. Harrison *et al.* [1989] conclude from a study of the Geophysical Fluid Dynamics Laboratory (GFDL) model simulation of the 1982-1983 ENSO event that zonal advection is likely dominant in the central ocean, but further east meridional advection may play a role also. Philander and Hurlin [1988] consider a heat budget of the entire tropical strip in the Pacific during the El Niño-Southern Oscillation (ENSO) 1982-1983 event and conclude that poleward advection and latent heat cause the region to lose heat.

Upper ocean temperature observations over the NPO are now dense enough to provide a raw quantitative estimate of heat content variability. However, the effects of advection are difficult to glean from the data alone since both direct and indirect velocity observations are inadequate in the NPO. It is therefore natural to attempt to supplement upper ocean temperature data and heat flux data with temperature and velocity fields hindcast by using an OGCM.

We here study the anomalous heat content variability in the Pacific Ocean observations together with a Pacific Ocean GCM hindcast in order to identify the mechanisms of variability. The model has previously been used by Miller *et al.* [1994a,b] to study the dominant oceanic processes involved in the 1976-1977 climate shift of the Pacific Ocean SST field and by Cayan *et al.* [1995] to study seasonal anomalies of SST patterns and processes. In this study we have improved both the forcing strategy for the model, which now results in more realistic monthly mean forcing, and the method of archiving the data, which yields precise evaluations of monthly mean heat content and the processes that control it.

We describe the model heat balance only in those areas where model and observed heat storages show a rea-

sonable correspondence in phase and amplitude. This is, of course, a necessary but not sufficient condition to validate the model heat balance. However, given the lack of a dense enough data set of observations we can do no better. In addition, we believe that the chances of getting the right heat storage from a wrong heat balance are very slim since we are computing regional averages in (dynamically) different regions across the Pacific Ocean. The good agreement between model and observations shown by Auad *et al.* [this issue] (hereinafter referred to as Part 2) for interdecadal timescales also points in the direction that the right heat balance is being simulated by the model.

Additional model-observation comparisons (to those shown in this paper) seem to indicate that the right heat storage was obtained from the right heat balance equation. For instance, the spatial structure and amplitudes of a 7-year time average of the surface horizontal heat advection term obtained from surface drifters in the tropical Pacific showed [Tropical Ocean Global Atmosphere (TOGA) Numerical Experimentation Group, 1995] good agreement with that one computed here from OPYC (model) data. Good agreement is also found with results obtained from previous modeling studies [e.g., Barnett *et al.* 1991, Miller *et al.*, 1994a,b]. Because a predominant time scale emerged (ENSO), we have bandpassed the fields to highlight the balances associated with this time scale in selected key regions. The interdecadal timescale is discussed in Part 2.

Our goal is to provide a first detailed qualitative and quantitative description of the anomalous heat balance in the upper 400 m of the NPO. Knowledge of the oceanic heat balance in a given region is crucial for the success of predictability studies, for the development of simplified models, and, most important for its diagnostic implications in climate changes and ocean-atmosphere interactions.

Section 2 briefly describes the ocean model and its forcing functions. Section 3 describes the temperature observations, while section 4 outlines the methods used to bandpass the time series and compute heat storages. In section 5 we present the results by first comparing the model and observed heat storages in the upper 400 m of the Pacific Ocean for interannual or ENSO timescales and then by showing the model heat balance for those areas where model and observed heat storages show a good correspondence. Sections 6 and 7 are left for discussion and summary.

2. The Model

The primitive equation ocean model, known as OPYC, was developed by Oberhuber [1993] and applied by Miller *et al.* [1994b] to study monthly mean through decadal-scale variations over the Pacific Basin (64°N to 76°S ; 120°E to 60°W). The model is constructed from eight isopycnal layers (constant potential density but variable thickness, temperature and salinity) that are fully cou-

pled to a bulk surface mixed-layer model. The resolution is relatively coarse; 4° in the midlatitude open ocean, though with (a) 0.5° north-south resolution at and near the equator and (b) 1.6° near the eastern/western equatorial boundaries, so only large-scale patterns can be considered with confidence. The surface forcing consists of a monthly mean seasonal cycle climatology of wind stress (Comprehensive Ocean-Atmosphere Data Set, COADS, and Florida State University, FSU, winds), total surface heat flux (COADS) and turbulent kinetic energy input to the mixed-layer (obtained from COADS and FSU winds), to which are respectively added the specified monthly anomalies from 1970-1988 derived from COADS observations. COADS winds were used outside the $\pm 20^{\circ}$ tropical band, while FSU winds were used inside it. COADS and FSU winds were smoothly blended in a 5° band at $\pm 20^{\circ}$. In the low-latitudes, between 20°S and 20°N , the anomalous heat fluxes are poorly known (and generally serve as a damping mechanism along the equator) so a Newtonian damping parameterization is used, whereby the SST anomalies are damped back to model climatology with 1 to 4 month timescales [see *Barnett et al.*, 1991, for a map of the coupling coefficient]. There is no SST feedback to the anomalous forcing so that the model is not constrained to reproduce the observed temperature variations. A thorough discussion of the model framework and forcing strategy is provided by *Miller et al.* [1994a,b] and *Cayan et al.* [1995].

The forcing strategy was modified from that of *Miller et al.* [1994b], in that we applied the technique of *Killworth* [1996] to properly allow linear interpolation of weighted monthly mean forcing anomalies (added to the seasonal cycle forcing). *Miller et al.* [1994b] did simple linear interpolation of the monthly mean forcing, which yields monthly mean model forcing typically weaker than the true monthly mean observed forcing. *Killworth* [1996] proposed increasing the input monthly mean forcing fields to allow linear interpolation yet cause the model to properly experience monthly mean forcing from the observations.

The complete model heat budget terms (see section 5.3) were saved as monthly means in each layer of the model. Postprocessing involved summing up the proper number of model layers to determine the heat budget in the upper 400 m of the water column. The heat budget balanced to within 1%. Further postprocessing (filtering and other procedures.) is discussed in later sections.

3. The Observations

3.1. The Temperature Data Set

The temperature data set consists of all available XBT, conductivity-temperature-depth (CTD) and mechanical bathytermograph (MBT) observations over the period 1955-1992 assembled and quality controlled by

the SIO Joint Environmental Data Analysis Center (JEDAC) (<http://jedac.ucsd.edu>]). Processing of the raw hydrographic data to obtain anomalous temperatures at several standard depths from the surface to 400 m is described by *White* [1995]. Since we wish to directly compare the data with a 1970-1988 simulation, we only use data from the 1970-88 time period which is also the best sampled time interval. A monthly mean climatology was computed for the period 1970-1988, and monthly temperature anomalies were defined with respect to that climatology. Temperature anomalies are then available at a series of standard levels to 400 m depth on a 5° longitude by 2° latitude grid. The original data set was obtained from ships of opportunity and the data were later optimally interpolated, in space and time, to the grid mentioned above.

3.2. Errors

In planning for the World Ocean Circulation Experiment, WOCE, errors in heat budget components averaged over large portions of the global ocean were estimated to be approximately 10 W m^{-2} , exceeding the expected interannual signals of 5 W m^{-2} . *White* [1995] discusses in detail the issue of interpolation errors and their minimization. Different types of errors affect our estimates of the heat storage fields. Sampling errors, in both space and time, are the main source of error that affect the observed field. The numerical model is subject to sampling errors as well since the atmospheric forcing functions (wind stresses and heat fluxes) are only estimates of the true forcing. Using model and data together, we estimate regional errors for interannual heat budget components in this study to be about $2\text{-}3 \text{ W m}^{-2}$. We discuss this important topic in section 5.

3.3. Methods

Model and observed heat storage were computed by integrating local heat storages in the upper 400 m of the Pacific Ocean,

$$H(x, y, t) = \sum_{z=-400 \text{ m}}^{0 \text{ m}} \rho_0 C_p T(x, y, z, t) \Delta z \quad (1)$$

where H is heat storage (in joules per square meter), x , y , and z are the east, north and vertical coordinates respectively, t is time, $\rho_0=1025 \text{ kg m}^{-3}$ is the reference density and $C_p=4180 \text{ J kg}^{-1} \text{ }^{\circ}\text{C}^{-1}$ is the constant heat capacity. T and Δz are the local temperature and depth interval respectively associated with that temperature (for the model Δz is a function of space and time). Observed temperatures are the results of linear interpolation, while model temperatures are the results of layered (quasi-Lagrangian) calculations (with only a fraction of the layer that intersects 400 m included in the evaluation of heat content). Once H is obtained for

both model and observations, the monthly mean climatological annual cycle is removed and the resulting time series is band passed in the frequency band of interest.

The 400 m level was chosen as the base level for heat storage for several reasons, the main reason being that the JEDAC temperature observations (mainly XBTs) used in this paper generally extend to no more than 400 m. However, in addition, integrating down to 400 m (1) helps to measure the amount of heat exchanged between the upper and deep oceans, (2) includes contributions coming from heat fluxes due to turbulent mixing processes characteristic of the mixed-layer's base and heat fluxes associated with isopycnal oscillations, and (3) allows us to compare our results with those of *White* [1995], who studied the temporal and spatial structure of heat storages integrated in the upper 400 m of the North Pacific Ocean.

The ENSO timescale was chosen since it is the most energetic frequency band (except for the annual cycle) of any of the variables studied herein. The chosen cutoffs of the interannual frequency band were 2.5 and 8 years, based on observed and modeled spectra that exhibit valleys at or near those two periods. The interannual timescale is well resolved in time by the monthly sampling rate of the model forcing functions. The band-passing procedure was carried out by using the Kaylor filter [Kaylor 1977], which has a variable cutoff frequency (selected by the user). The filter does not introduce any phase shift in the data and has a remarkably steep cutoff slope. We tested the skill of our filter by computing the cross-spectral analysis between some time series after and before filtering them in the 2.5 to 8 year band. In this band the phase and amplitude of the transfer function were always very close to 0 (smaller than 10°) and 1 (between 1.1 and 0.9), respectively, and the coherence was close to 1 (higher than 0.9).

The basic procedure followed in this paper is as follows. First, we compare model heat storages with those computed from observations. Second, for those areas where we obtain a reasonable model-observation comparison we describe the model heat balance.

4. Results

4.1. Modeled and Observed Volume-Integrated Heat Storages

Heat storage anomalies were computed for the period 1970-1988 in the upper 400 m of the Pacific Ocean from both model and observed data. Time series of area-averaged unfiltered heat storage anomalies for the regions north of 24°N and north of the equator showed high model-data correlations (0.83 and 0.72, respectively) with the variance dominated by both ENSO and decadal timescales. The correlations imply that the amount of heat being pumped into or extracted from these volumes, either horizontally or vertically,

produces similar changes in the total heat content of the volume for both model and observations. Our 2.5 to 8 year band-passing technique is used to quantify skill in the dominant ENSO frequency band. The analysis of decadal timescales, periods longer than 8 years, is presented in Part 2. Basinwide averages have no information regarding the horizontal distribution of heat storage over the domain under study. In the next section, pointwise analyses of heat storage are presented along with analyses for specific areas, or "boxes", typically 10° by 20° in size and 400 m deep, where the model-data correlation is high.

4.2. Modeled and Observed Local Band-Passed Heat Storages

The heat storage data sets were treated by first removing the monthly mean climatology and then band passing in the frequency bands of interest. Basic statistical analyses were carried out for the time series of each grid point on the respective grids for the model and observed data. The comparisons and analysis will be mainly concentrated in the NPO because of its more dense XBT-CTD sampling than that in the South Pacific. To include the whole equatorial band, our maps (see below) are constructed from the 20°S parallel northward.

Plate 1 shows heat storage fields of the upper 400 m for the ENSO timescale from July 1981 to July 1984 (6-month intervals), which included the large 1982-1983 ENSO event. Model and observed heat storage anomalies show a remarkable agreement in both tropical and extratropical regions. The main discrepancy between the model and observed fields is observable along the coast of Central and North America, where the coastally trapped poleward propagating signals in the model are weaker and somewhat slower than those in the observations. This finding is very likely due to the coarse horizontal resolution of the model. The observation and model (Plate 1) seem to suggest a poleward penetration to the extratropics through coastally trapped Kelvin-like wave signals along the eastern boundary. Wind stress curl-model heat storage correlations are not significant (not shown) and indicate that local wind stress curl forcing is not an important local driving agent along the eastern boundary. However, our wind data are smoothed to synoptic scale and do not include the small-scale winds typical of the coastal ocean. *Miller et al.* [1997] find that the modeled interior ocean response is a combination of the static thermocline response to a large-scale pattern of Ekman pumping plus a train of westward traveling Rossby waves, which account for the greater part of the ENSO-scale propagating thermocline fluctuations. In addition, they found that a remotely forced component is prominent near the eastern boundary, but this only contributes weakly in the model open ocean. The model-observation comparison

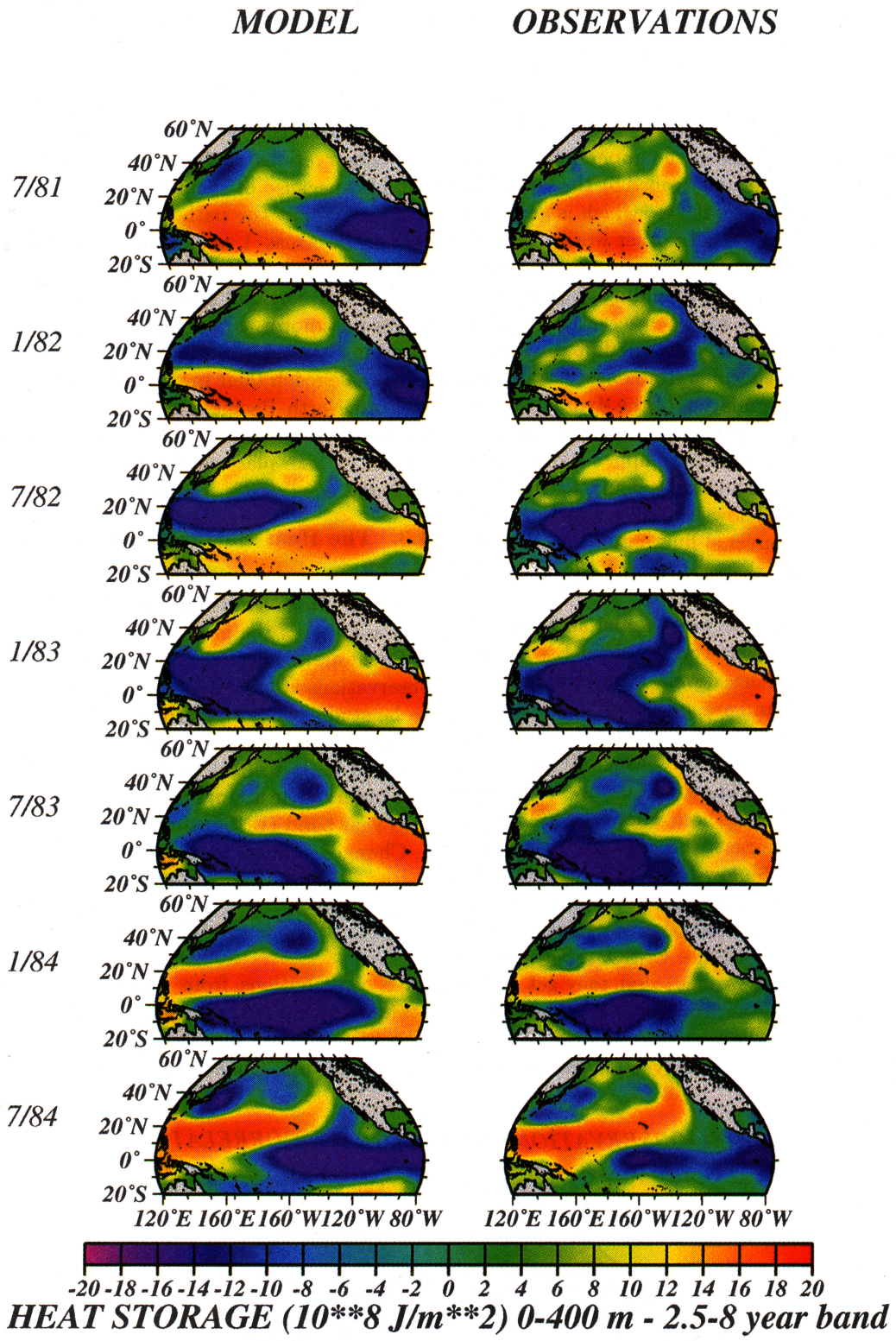


Plate 1. Model and observed heat storage anomalies for El Niño Southern Oscillation (ENSO) timescale (2.5–8 years).

for other years in the time span 1970–1988 exhibit a similar degree of visual correlation.

The heat storage in the upper 400 m of the tropical and low-latitude Pacific exhibits a behavior in good agreement with previous descriptions [e.g., Philander, 1990] of the ENSO phenomenon. The early stages of

the strong 1982–1983 El Niño event can be seen in July 1981 (Plate 1) when large positive anomalies are mainly concentrated on the western equatorial Pacific Ocean. These anomalies move eastward along the equatorial band and, after reaching the coast of South America, propagate poleward along the coasts of North and

South America (though not as efficiently in the model). Then, westward propagating Rossby waves (July 1983), seen as northeast-southwest elongated positive anomalies, start to develop and carry positive anomalies to the western part of the subtropical North Pacific Ocean.

The heat storage anomalies in the upper 400 m of the midlatitude NPO are largely controlled by the lower half of the volume (i.e., 200 m to 400 m, which is generally below the winter mixed-layer). In other words, thermocline fluctuations contribute the greatest variations to upper ocean heat content. This finding suggests that the agreement found in the model-observation comparisons is not simply controlled by model diabatic surface boundary conditions as specified from observations, but rather to a reasonable simulation of the dynamical contribution to interior heat fluxes. (The reader can make a comparison of heat storage in the upper 400 m versus temperatures at different levels by going to the URL address given above.) Below we will explore this dynamical effect of the isopycnal fluctuations on the heat content, as well as the thermodynamic effects on the heat balance.

Correlation coefficients between model and observed heat storages (Figure 1) were computed for ENSO time scales. The 90% confidence levels were computed according to *Davis* [1976] and are, on a spatial average, 0.5 for the ENSO timescale. Areas of highest correlations (light areas) are patchy over the basin but organized by the types of responses known to occur. The areas of maximum correlation are those where the ENSO signal is known to be strongest, the equatorial strip, the northeast Pacific, and the low-latitude western boundary regions. At some locations such as the western mid-latitude regions, the low-correlation areas can be interpreted as areas where both the ENSO signals are so weak (in model and observations) that they get lost in the background noise. Other sources of low correlation between model and observations were mentioned above (e.g., model resolution and unresolved physics and sam-

pling errors (in space and time) in the observed field and forcing functions)

On the basis of the pointwise correlation maps, six different areas were chosen to study heat storage balances. These areas were not only selected because of the high observations-model correlations for heat storage but also because of their strategic location with what is known about the path followed by ENSO signals in the NPO. Areas 1 and 2 are located at the western and eastern ends of the equatorial waveguide. Area 3 is in the corridor along which thermocline Rossby waves are known to propagate westward. Area 4 is located in the center of the NPO subtropical gyre where isopycnals reach their maximum depths. Areas 5 and 6 (central North Pacific and California Current system) are located where maximum ENSO SST amplitudes are known to take place in the North Pacific Ocean [e.g., *Pan and Oort*, 1983; *Alexander*, 1992].

4.3. The Heat Balance in the North Pacific Ocean

4.3.1. Introduction. On the basis of the correlation analysis of the previous subsection we selected six different areas where the agreement between model and observations is favorable. Figure 2 shows the six areas to be studied below. In these regions we will compare the model and observed heat storages and break down the heat budget of the model. For each area the model and observed heat storages were band-passed in the 2.5 to 8 year band (ENSO timescale).

Changes in heat storage,

$$\frac{\partial H}{\partial t} = (\rho h \frac{\partial T}{\partial t} + T \frac{\partial \rho h}{\partial t}) C_p \quad (2)$$

have contributions from diabatic and adiabatic processes, where h is the depth interval or layer thickness. The first ones are due to changes in temperature only (second term). The second ones are due to changes in

MODEL-OBSERVATIONS HEAT STORAGE CORRELATIONS

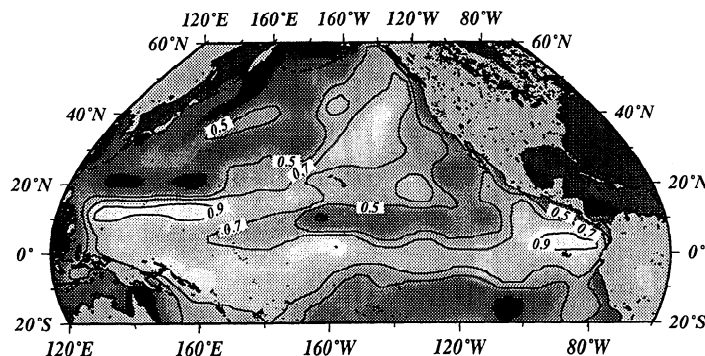


Figure 1. Correlation coefficients between model and observations of heat storage in the upper 400 m for ENSO timescales. Only the 0.5, 0.7, and 0.9 contours are drawn. The spatially averaged 90% confidence level is 0.5.

mass only (last term) and are sometimes called "thermocline heave." For a fixed volume, as in our case, the net effect of the latter term is through a flux of water, having a fixed temperature, through the base of the volume, i.e., the 400-m level. In this paper we describe the time and spatial fluctuations in heat budget components that result from both effects together and those caused only by diabatic processes. From (2) the adiabatic contribution is the difference between the total heat change minus the diabatic contribution. From now on we will refer to the three terms in (2) as the total, diabatic, and adiabatic heat balances from left to right, respectively.

The model heat equation is represented for each layer by,

$$\frac{\partial H}{\partial t} = \text{div} + VT_{400} + Q + H_{mix} \quad (3)$$

where for each term we use units of watts per square meter, Q is the surface heat flux, VT_{400} is the total vertical transport crossing the 400-m level due to both vertical heat transport associated with the three-dimensional divergence of the heat flux vector (i.e., $w\rho C_p T$, where w is the vertical velocity) and to cross-isopycnal mixing, div is the horizontal divergence of the heat flux, and H_{mix} is the horizontal mixing. Note that the words "vertical" and "horizontal" actually mean cross- and along-isopycnal, respectively, in the model.

In the model the second term in (2) is represented by

$$\rho h C_p \frac{\partial T}{\partial t} = \text{adv}_x + \text{adv}_y + V_{mix} + Q + H_{mix}, \quad (4)$$

where T is temperature, adv_x and adv_y are the zonal and meridional components of the horizontal advection of heat, respectively, and V_{mix} is the cross isopycnal mixing. The heat and temperature equation terms corresponding to each isopycnal layer are accordingly

band-passed, and (1), (3) and (4) are integrated in the upper 400 m and for the areas shown in Figure 1.

As we mentioned above, the 400 m depth was chosen because it is the deepest level reached by the observations maintained at the JEDAC and also because it is well beyond the reach of the turbulent effects that characterize the base of the mixed-layer. Choosing a fixed reference level, instead of a given isopycnal, is desirable if one wants to study contributions to the heat equation from propagating signals or, more generally, from any motion associated with isopycnal oscillations. We allow these motions to affect (3) since we are interested in providing a complete description of the heat balance that includes all contributions from vertical (oceanic) heat fluxes and also to compare with the 400 m integration done of *White* [1995]. To determine how important the contribution from isopycnal oscillations is to (2), we also computed the heat balance (3) integrated down to layer 4 of OPYC which has bottom depths ranging from 200 to 500 m, depending on the geographical location. The comparison for each box between both vertical integrations gave nearly identical results, because the main contribution to heat budget components come from the four upper layers of the model. This fact implies that we are trapping, in our vertical integrals, the strongest part of the signal in question.

4.3.2. Description of the total heat balance. Figure 3 shows the average box temperatures (the average temperature obtained by using all temperature values that fall inside the selected boxes of Figure 2) from both model and observations for areas 1-6. Typical periods of 3-4 y are seen from simple visual inspection of these time series. This is not an artifact of the band-passing technique, as the same periodicity is visually observed from nonfiltered temperature anomalies (not shown) for all areas. Maximum variability, i.e., maximum standard deviations, takes place, for both model and observed box temperatures, at both equatorial regions, areas 1 (0.21 °C for the observations) and 2 (0.23 °C), while for the remaining areas these

ANALYZED AREAS

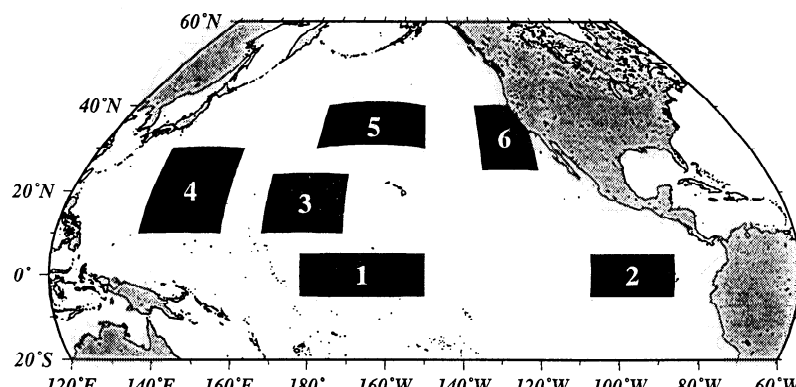


Figure 2. Selected areas where temperatures and heat budget components are averaged

values are smaller than 0.12°C . Poor heat storage comparisons were obtained for the Kuroshio region, since the model horizontal resolution fails to accurately resolve the western boundary current, and for the Gulf of Alaska, where motions such as coastally trapped waves and the Alaskan current have spatial scales much smaller than the horizontal grid size.

From these figures it is possible to track down individual events knowing the main propagation path of the ENSO temperature anomalies [e.g., Philander 1990], which can also be appreciated from our Plate 1. For instance, in area 4 (Figure 3) (western subtropical Pacific) and in mid-1984, both model and observations show an absolute maxima of about 0.4°C for the 1970-1988 period. It takes about 20 months for this signal to reach area 1 (western equatorial Pacific). From there it takes another 4-5 months (6 months is the travel time estimated from model SST data by Barnett *et al.* [1991]) to reach the coast of South America, area 2, and an extra 2-3 months to get to the California Current system region (area 6). The travel time of the positive anomalies from east to west (lower panels in Plate 1) across

the subtropical NPO is about 12 months. Below we will relate these anomalies to westward propagating Rossby waves and find out that along their path, heat content time fluctuations are dominantly caused by isopycnal heave. Thus the overall cycle takes about 3.3 years to be completed, which is the periodicity observed from the time series in Figure 3. Similar descriptions, in terms of the travel times just mentioned above, are valid for other events present in the time series of Figure 3. The time series corresponding to the terms of the heat budget (3) are shown in Figure 4 for areas 1-6. Even though our areas are very different from those defined by White [1995], the model heat storages and time change of heat storage show amplitudes and timescales that visually agree with those reported by White.

From historical observations it is known that areas 1 and 2 (western and eastern equatorial regions, respectively) are characterized, in general, by strong wave activity, which mainly propagates in the zonal direction. On interannual scales they are characterized by large variations in their heat content in relation to the extratropical areas discussed below.

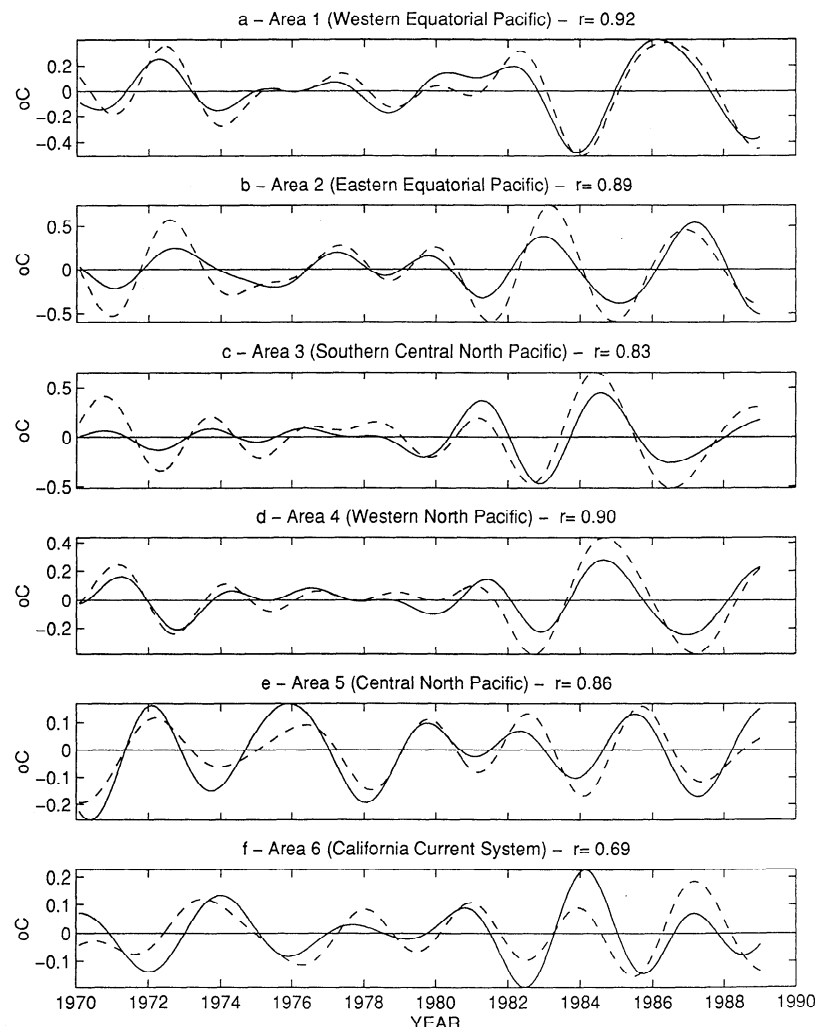


Figure 3. Model and observed average box temperatures for ENSO timescales in the upper 400 m. Correlation coefficients (zero lag) between both time series are shown at top.

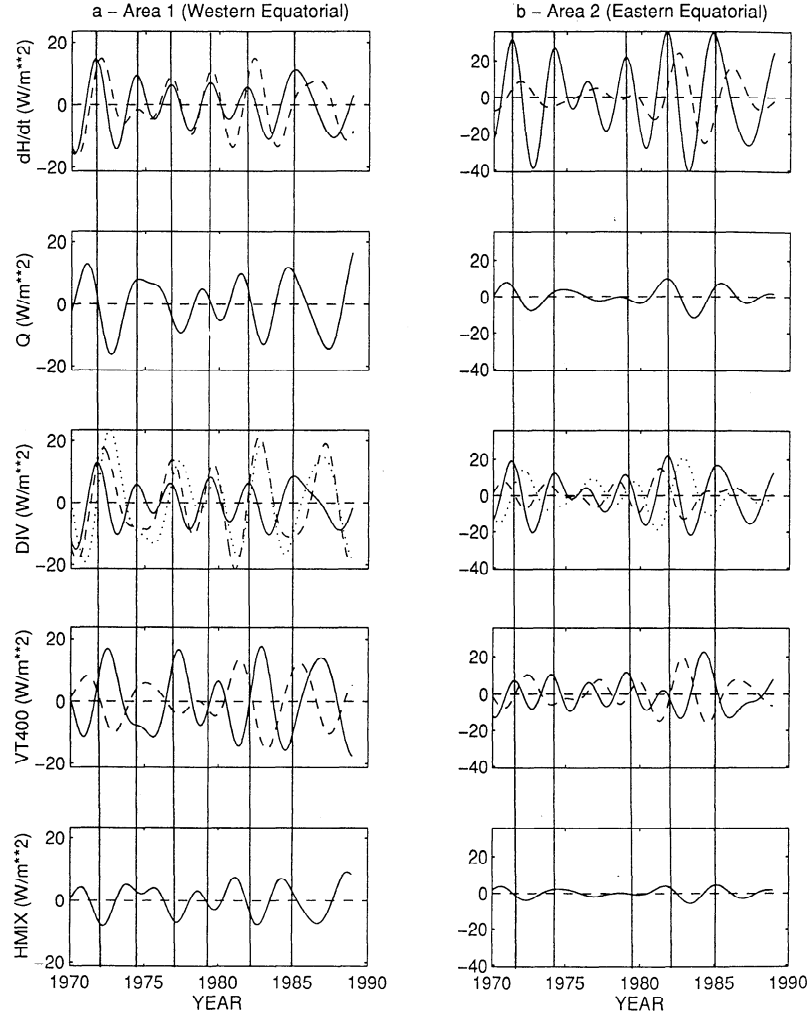


Figure 4. Spatially averaged time series of the OPYC total and diabatic heat budget components (as in (3) and (4), respectively) for area (a) 1, (b) 2, (c) 3, (d) 4, (e) 5, and (f) 6. In the top panel dH/dt is represented by a solid line and is the total time change of heat shown both in (2) and (3). The dashed line is the diabatic contribution to dH/dt . The surface heat flux and horizontal mixing terms are the same for both equations. In the *div* diagram the solid line represents the total divergence of the heat flux (as in (2)), respectively, and the dashed and dotted lines represent the zonal and meridional advection contributions to that divergence. The solid line in VT_{400} is the vertical transport of heat at 400 m coming from both the vertical heat transport due to the oscillations of the isopycnals ($w\rho C_p T$) and cross-isopycnal mixing. The dashed line is the contribution from cross-isopycnal mixing to VT_{400} . Positive and negative values imply warming and cooling respectively.

Figure 4a shows the heat balance for area 1. The solid lines refer to the total heat balance implied by the first term in (2). The dashed lines are the diabatic contribution implied by the second term in (2). This latter balance is examined in detail in the next subsection. All terms shown in (3) make comparable contributions to the total heat budget with horizontal mixing being the smaller contributor. The time change of heat is in phase with the divergence term *div*, while the surface heat flux is in opposite phase with the vertical heat transport VT_{400} . Different events in the time series show very similar heat balances. Figure 4b shows the heat balance for area 2 (eastern equatorial). The heat budget shown in (3) can be simplified to

$$\frac{\partial H}{\partial t} = \text{div} + VT_{400} \quad (5)$$

where the last two terms, for a given time, add up to account for the variability of the time change of heat (top panel). Again, as in area 1, different events show similar heat balances.

One major difference in the heat budget of these two equatorial areas is the weaker role of Q in the easternmost area. Since Q is proportional to anomalous SST by approximately a factor of $10 \text{ Wm}^{-20} \text{C}^{-1}$ in both regions [Barnett et al., 1991], the model SST anomalies are somewhat smaller in area 2 than in area 1. Yet the advective and mixing effects are markedly larger in

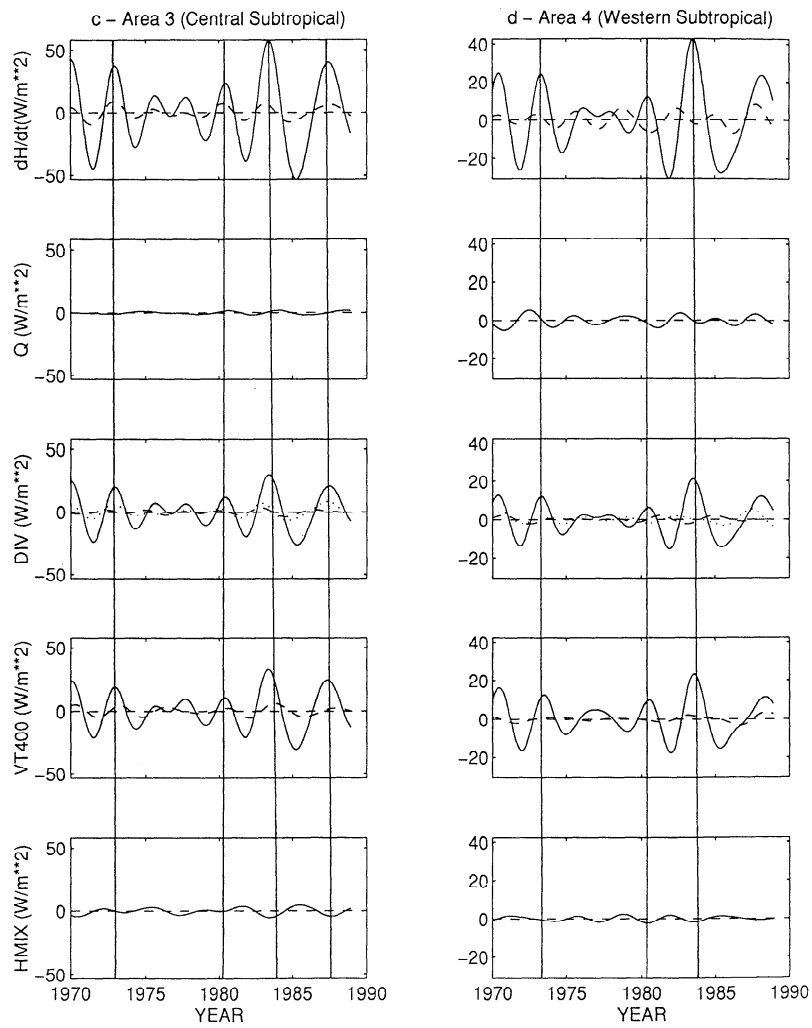


Figure 4. (continued)

region 2, where both the mixed-layer and thermocline depth tend to be shallower.

Area 3 was selected because it is located on the corridor along which warm anomalies propagate westward in the form of Rossby waves (see Plate 1) for ENSO timescales. It is located on the zonal axis of the NPO subtropical gyre and some 30° eastward of its center. As for area 2, the heat balance in area 3 can be also reduced to (5). However, it should be noted that since Q only represents a damping mechanism for SST here (as a result of poor observations), the diabatic effects are likely to be underestimated in importance. On the other hand, this area is where the largest heat budget component amplitudes are found, suggesting the dominance of adiabatic processes nonetheless. Different events in the time series of $\partial H/\partial t$ are made up from the joint contributions coming from the horizontal divergence of the heat flux and the vertical heat transport.

Area 4 (western North Pacific) is located in the center of the NPO subtropical gyre, where maximum isopycnal depths are historically observed. This area is characterized by active Ekman pumping. Figure 4d shows the heat balance corresponding to area 4. Like area 3, area

4 is also dominated by adiabatic processes, and its main balance can be reduced to (5). In both areas 3 and 4, div and VT_{400} are in phase with $\partial H/\partial t$. Since vertical mixing is small at 400 m, this balance states that three-dimensional divergence of the heat flux is the dominant mechanism responsible for changing the heat content in these areas. Thus warming events are associated with a deepening of the isotherms and vice versa (with the caveat that heat flux forcing is not included in the model in this region because of sparse observations).

Area 5 (central North Pacific) is located on the northern flank of the North Pacific subtropical gyre, and its heat balance is shown in Figure 4e. Diabatic processes contribute substantially to the time changes of heat, while the total vertical transport of heat at 400 m is dominated by contributions resulting from the oscillations of the isopycnals. All heat budget components make important contributions to the local heat change, $\partial H/\partial t$. The heat balance of this area can be somewhat simplified to one between the local change of heat, the net surface heat flux, and the vertical transport of heat at 400 m, which here is almost entirely due to isopycnal oscillations. This is true not only because the horizon-

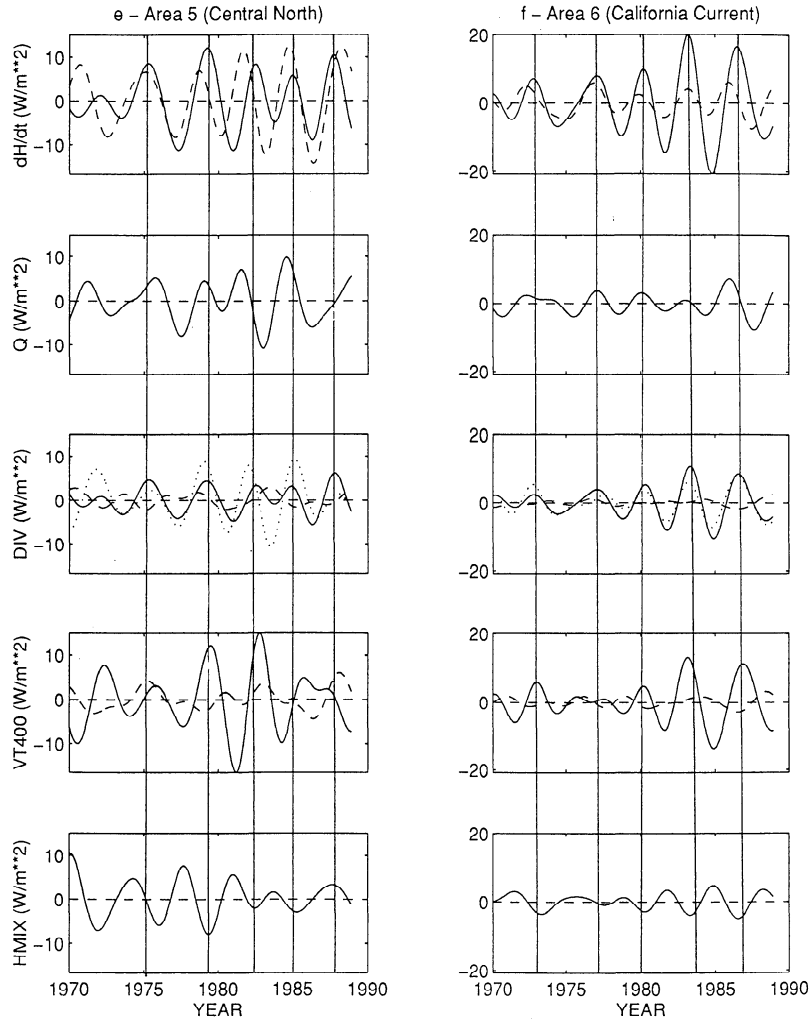


Figure 4. (continued)

tal divergence of the heat flux and the horizontal mixing are smaller (weak gradients), but because these last two terms tend, in general, to cancel each other. Warming episodes (positive peaks in the top panel of Figure 4e) are thus caused by vertical heat transfers, both through the ocean surface and through the 400 m level (downwelling). The signs of these three time series reverse for cooling episodes.

Area 6 occupies the eastern edge of the NPO subtropical gyre, i.e., the California Current system region. The heat balance of area 6 (Figure 4f) can also be simplified to (5). The first 8 years of the $\partial H/\partial t$ time series show dominance of diabatic processes while adiabatic processes are dominant from about 1978 to 1988, mostly because of an increase in the vertical transport of heat associated with the oscillations of the isopycnals at the 400-m level. Different warming (cooling) events are all caused by the three-dimensional divergence (convergence) of the heat flux.

The maps of Figure 5 show the different heat equation (3) terms at 4-month intervals starting in May 1982. The very gross feature to note is that on a local basis the heat balance can be simplified to one between the

time change of heat and the three-dimensional divergence of the heat flux. In May 1982 the eastern half of the tropical Pacific is warming up (positive values, i.e., solid contours), while the western half is cooling off as the positive anomalies travel eastward (compare also with Plate 1). The warming along the eastern boundary moves poleward (September 1982 and January 1983) and is associated with heat flux divergence and vertical processes of waves and wind curl forcing [Miller et al., 1997]. In the mature stages of this ENSO event (January 1983) the western subtropical Pacific is warming after the arrival from the east of heat flux divergence effects from westward propagating Rossby waves. At almost all locations a positive (negative) $\partial H/\partial t$ is accompanied by downwelling (upwelling) and a divergence (convergence) of the heat flux.

In the next subsection we study the diabatic contributions to heat storage changes (second term in (2)). These contributions are interesting in themselves since they are the ones that can directly respond to the external (observed) forcing Q . In contrast, the adiabatic contributions [last term in (2) and inferred as the difference between the solid and dashed curves in the top panels

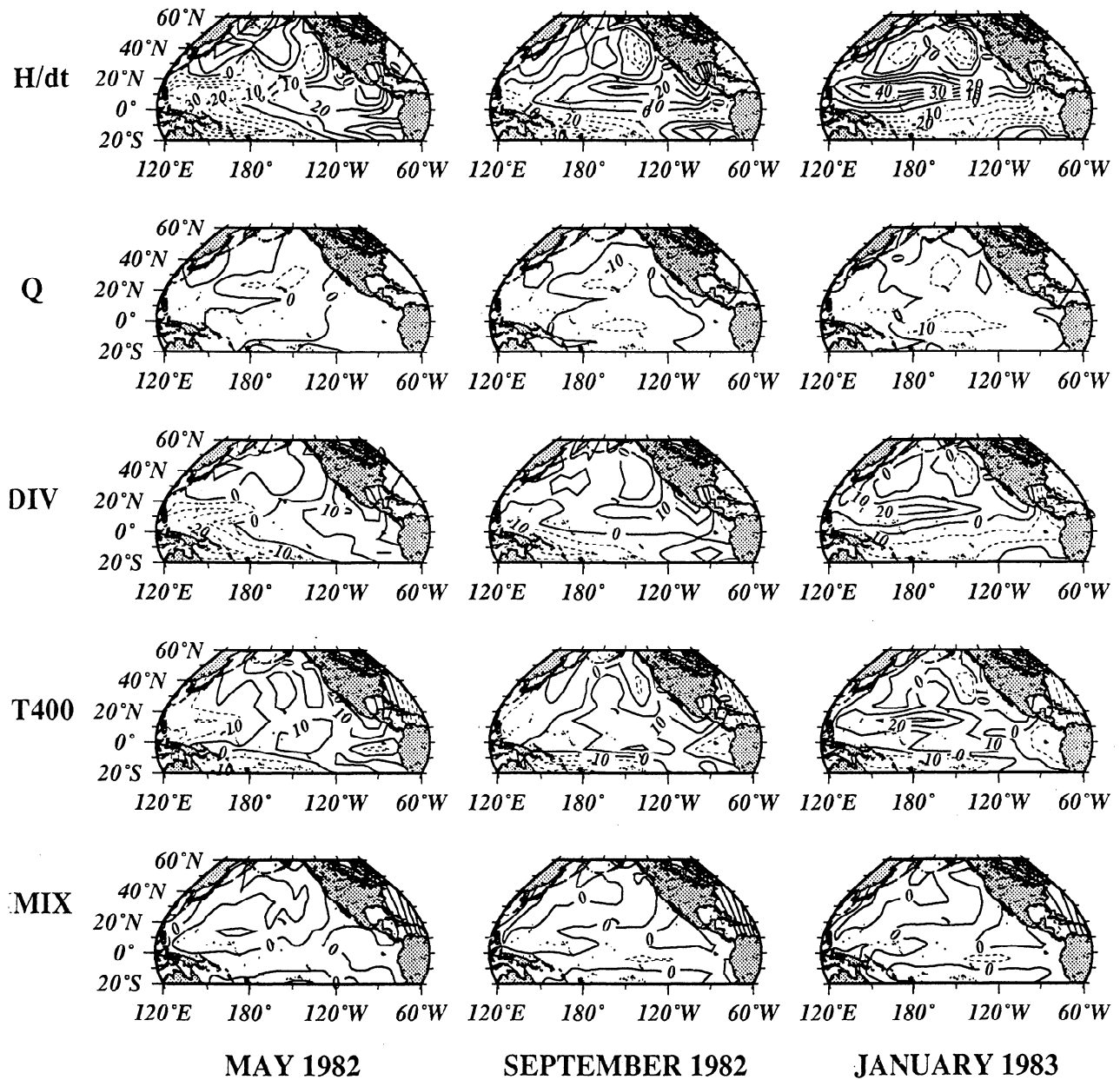


Figure 5. Time sequence of the spatial structure of the total heat budget components for ENSO timescales. The contour interval is 10 W m^{-2} , being the maximum and minimum contours +40 and -40 W m^{-2} . The reader should be careful in looking at this figure, since it is tempting to draw conclusions about the heat balance for any area, and not all areas showed a good agreement between model and observations. Plate 1 and Figures 2 and 4 show model-observation comparisons that indicate what areas are reliable for drawing any conclusion about the heat balance in the North Pacific. At any rate, and as we mentioned in the text, some of the low correlations estimated between model and observations (e.g., 5° north of the equator and east of the dateline) are probably due to low spatial (and temporal) sampling [see White, 1995].

of Figure 4] respond to the wind stress curl and inertial effects through the vorticity equation. Before proceeding with the description of the temperature balance we quantify the relative importance of the adiabatic to the diabatic contribution. These ratios are shown in Figure 6. Areas that are occupied by the southwestward extending positive anomalies most visible from the two bottom panels of Plate 1 and very likely associated with westward propagating thermocline Rossby waves have the largest ratios, probably as a result of the large

excursions experienced by the isopycnals as thermocline Rossby waves propagate westward on ENSO timescales. Moreover, areas having ratios higher than 2 show a total heat balance that can be simplified to one between the time change of heat and the three-dimensional divergence of heat, and this is linked to the Rossby wave activity mentioned above.

4.3.3. Description of the diabatic contributions to the total heat balance. In this subsection we will describe the temperature equation (the diabatic

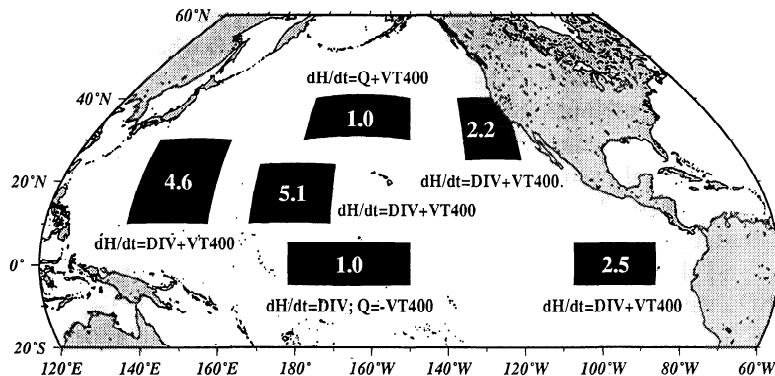


Figure 6. Ratios between the adiabatic and the diabatic contributions (last two terms in (2)) to total heat change, i.e., $T\Delta h/h\Delta T$. These ratios were obtained from the standard deviations of the time series shown in of Figure 4. Also shown is the dominant heat balance corresponding to each area. Note that the ratios higher than 2 have implicit a balance between the $\partial H/\partial t$ and the three-dimensional divergence of the heat flux

contribution to the total heat budget) only for those areas where Figure 6 shows ratios lower than 4, i.e., where the total heat balance has an important contribution from diabatic processes. Figures 4a and 4b show the diabatic heat balance for areas 1 and 2. The balance shown in (4) can be only slightly simplified by excluding the horizontal mixing term. Unlike the extra-tropical areas, all terms make important contributions to the total heat budget of these two equatorial areas (consistent with SST budget results discussed by *Miller et al.* [1993] for an earlier version of OPYC). For both areas the zonal and meridional components of the heat advection term ($\rho C_p \mathbf{V} \cdot \nabla T$, where \mathbf{V} is the velocity vector) make important contributions to the total divergence of the heat flux vector (div). In area 1, the zonal and meridional contributions to the heat advection term have comparable amplitudes and the same sign. Area 2 also shows zonal and meridional advection having comparable amplitudes but with opposite signs. This finding is likely due to area 2 being mainly remotely driven by waves while local wind forcing is more prominent in area 1. For both areas, cross-isopycnal mixing makes a significant contribution to the total vertical heat transport (row labeled VT_{400}). For both areas, V_{mix} is 180° out of phase with respect to $w\rho C_p T$ and implies that the mixing mechanism tends to smooth vertical gradients created by the vertical transport due to the rising and falling isopycnals.

In the western equatorial Pacific (area 1), different events are controlled by similar physics. However, note that the strong ENSO event of 1986-1987 has a much longer duration (top panel of Figure 4a) than the stronger 1982-1983 ENSO. This longer, though weaker, warming period in 1986-1987 seems to be the result of the combined action of different processes acting at once, since there is not one single term that balances by itself the time change of diabatic heat (second term in (2)).

Area 2 (eastern equatorial) also shows a longer but weaker warming period for the 1986-1987 ENSO event compared to the 1982-1983 event. For this area the warming period seems to be mainly driven by down-welling. The 1986-1987 event seems also to be different in comparison with the 1972-1973 and 1982-1983 events in that is the only event showing a minor warming contribution from the zonal flow and little influence of the meridional flow. Area 2 has important contributions from vertical mixing processes to the temperature budget, which, unlike area 1, are more or less in phase with the times of maximum external warming. *Barnett et al.* [1991] also report active vertical mixing processes in the eastern equatorial Pacific when the warm anomalies reach the coast of South America.

Areas 5 and 6 are similar in that their diabatic heat balances (Figures 5e and 5f) can be mainly reduced to

$$\frac{\partial T}{\partial t} = adv_y + Q + H_{mix} \quad (6)$$

Miller et al. [1994a] find that SST anomalies in area 5 are predominantly controlled by surface heat flux forcing and vertical mixing with a weaker contribution by horizontal advection. In area 6, *Miller et al.* [1994a] found that surface heat fluxes alone are the dominant driver of SST. The diabatic heat content, in contrast, in both the central and eastern Pacific regions is controlled by surface heat fluxes and north-south advection, with vertical mixing playing a minor role. Both areas are damped moderately by horizontal mixing, which is almost in quadrature with the warming-cooling time series (top panel). Meridional advection in area 5 is larger than both zonal advection and the total divergence of the horizontal heat flux. Thus, an important contribution to the div term is being made by the horizontal divergence of the mass flux (i.e., difference between the solid line and the sum of the dashed and dotted lines).

In area 6 (California Current) the horizontal divergence of the heat flux is largely dominated by the meridional advection of heat. For both areas 5 and 6 the cross isopycnal mixing makes a minor contribution to the total vertical heat transport (which is mainly affected by vertical advection). All interannual events in both areas show similar heat balances. For all areas the typical time period of the heat budget components ranges between 3.0 and 3.8 years, and there is strong variability during times when ENSO events are not active in the tropics.

A time sequence of the spatial structure of heat budget components for the 1982-1983 event is shown in Figure 7. In May 1982 (early stages) and in the tropical strip, $\pm 10^\circ$, zonal advection dominates the heat balance. The midlatitudes are mainly dominated by Q , the surface heat flux that cools off the central NPO [e.g., Alexander, 1992] and warms up the Kuroshio area. Vertical mixing is important in the eastern tropical Pacific. In September 1982, tropical areas, Q and V_{mix} show both an increased cooling which seem to be compensated by an increased warming by meridional advection. The midlatitudes are still controlled by the surface heat flux. Note that as the ENSO event progresses in time, the meridional advection and the vertical mixing terms become more important in the tropics and in midlatitudes (January 1983). This latter is partly in agreement with the findings of Battisti [1988], who uses a coupled atmosphere-ocean model and finds meridional advection playing an important role in SST evolution in the eastern portion of the equatorial Pacific, and of Barnett *et al.* [1991], who find vertical heat transport processes to be important in the eastern tropical Pacific. However, now the damping effect (through Q) is maximum at the tropics because of the large positive SST anomalies present there. In January 1983, maximum heating takes place at the far eastern tropical Pacific, and this is balanced mainly by vertical transport of heat. In the central equatorial region the diabatic heat balance is complicated in the sense that all terms but horizontal mixing have large amplitudes. The midlatitudes are still being cooled off by the surface heat flux and meridional advection and warmed up by a mild horizontal mixing.

5. Discussion

Observed ENSO timescale heat content variations are well matched to our simulated heat content variations for many regions of the Pacific. We therefore studied these heat content variations in key regions of a simulation of the Pacific Ocean. The total heat balance revealed the smaller role played by the surface heat flux Q as compared to the diabatic heat balance. Thus, the overall fluctuations in heat storage of the upper 400 m in the NPO are mostly controlled by the divergence of the three-dimensional heat flux. The only area where Q has a key role in determining the amount of total heat in the upper 400 m is the central NPO (area 5),

where the vertical advection of heat is the other main contributor (rather than total divergence of the heat flux). We conclude that one of the reasons we obtain such a good comparison between observed and modeled heat storages in the central NPO (area 5), even though the model coarse grid is far from resolving the Kuroshio system located to the west of area 5, is that zonal advection plays a minor role there. Q is somewhat important in the equatorial area, but there its role is to damp and not to force the heat anomalies.

A substantial difference was found between the diabatic heat balance in tropical and extratropical regions for ENSO timescales. In the extratropical regions (our areas 5 and 6) the main balance can be reduced to one between the time change of diabatic heat, the external heat flux forcing, the meridional advection of heat, and horizontal mixing. At these latitudes the surface heat flux Q and the meridional advection contributions are of crucial importance in understanding the oceanic-atmospheric connection. The model response is dominated by meridional current fluctuations advecting the mean north-south temperature gradient, rather than mean advection of temperature anomalies. The relatively smaller amplitude of the zonal advection term in the extratropical areas is due to the absence of strong east-west temperature gradients (when anomalous currents contribute to the balance) and the absence of strongly subducting temperature anomalies (when mean advection contributes) in comparison with the observations [Deser *et al.*, 1996]. The relatively smaller amplitude of the vertical heat flux at 400 m (with respect to the tropical areas) is probably due both to a decreased response of the vertical heat flux to a decreased zonal advection and to the fact that at midlatitudes isopycnal oscillations take place at shallower depths than they do at the tropics (both above the 400 m level).

In the tropical regions (our areas 1 and 2) all diabatic heat budget components show comparable amounts of variance. In this respect, Barnett *et al.* [1991] use SST data from two different numerical models and point out that ENSO events in the ocean result from a complex interplay between several processes such as remote propagation of waves and local ocean response. The meridional heat transport for ENSO timescales in the central and western equatorial Pacific has a key role in closing the diabatic heat budget in the upper 400 m and when it is averaged over areas roughly 10° by 20° . However, maps showing the diabatic heat budget component's fields suggest that the size of the meridional advection term is smaller than its zonal counterpart. This finding is in agreement with some authors [e.g., Philander and Hurlin 1988], who do a top-to-bottom integration for the 1982-1983 El Niño, but in disagreement with others [e.g., Gill 1983, who does an analysis of SST for the 1972-1973 El Niño]. Thus the relative sizes between the zonal and meridional advection terms for area 2 (seen from Figure 4b in dashed lines) can de-

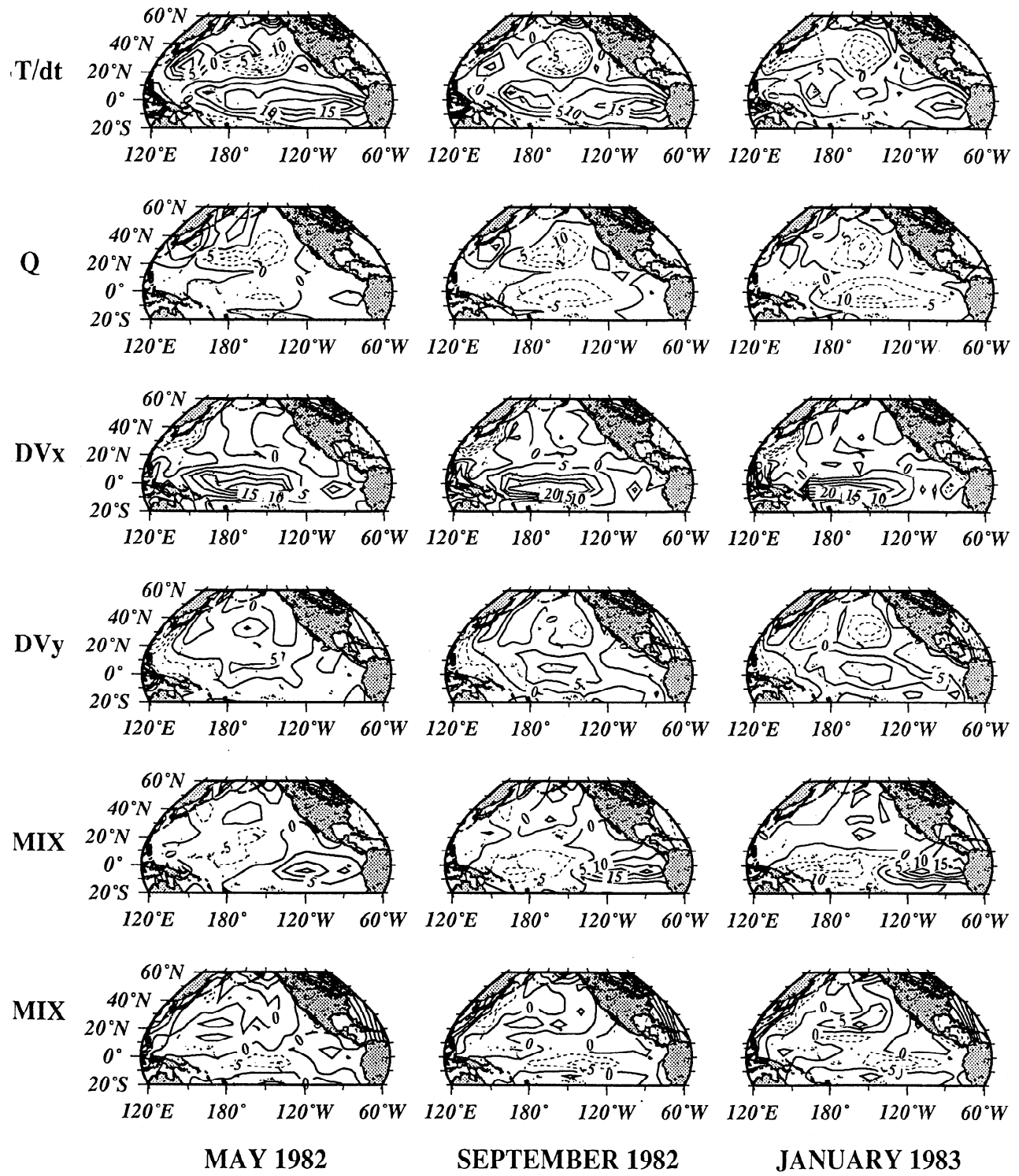


Figure 7. Time sequence of the spatial structure of the temperature equation components (i.e., the diabatic contribution to the total heat budget) for ENSO timescales. The contour interval is 5 W m^{-2} , being the maximum and minimum contours $+20$ and -20 W m^{-2} . The reader should be careful in looking at this figure, since it is tempting to draw conclusions about the heat balance for any area and not all areas showed a good agreement between model and observations. Figures 2, 4 and 6 show model-observation comparisons that indicate what areas are reliable for drawing any conclusion about the heat balance in the North Pacific. At any rate, and as we mentioned in the text, some of the low correlations estimated between model and observations (e.g. 5° north of the equator and east of the dateline) are probably due to low spatial (and temporal) sampling [see White, 1995].

pend on the regional averaging. It is also possible that the above discrepancy with the work of Gill is only due to the fact that this study and in the one by Philander and Hurlin, vertical integrals of the heat content are considered, as opposed to the SST analysis of Gill.

The anomalous heat budget was not sensitive to changes in the bottom limit of our vertical integration of the heat budget components, i.e., heat storages and heat budget components were computed down to 400 m and down to the fourth isopycnal, which depth varies between 200 m (high latitudes) and 500 m (center of the subtropical gyre) and almost identical results were obtained. The reason for this similarity is that the main part of the signals are concentrated in the upper 200 to 300 m of the water column.

Typical amplitudes of the anomalous time rate of change of upper ocean heat storage averaged in each box for model estimates (top panels in Figure 4) are approximately $\pm 10 \text{ W m}^{-2}$. This variability is balanced in OPYC with similar amplitudes of anomalous air-sea fluxes and heat transport divergences averaged over the boxes (remaining panels in Figure 4). This finding indicates that relative errors in anomalous time rates of change in heat storage, air-sea heat fluxes, and horizontal heat transport divergences of $\pm 2\text{-}3 \text{ W m}^{-2}$ were achieved in our attempt to close regional heat budgets. *White and Tai* [1995] demonstrated that the broadscale XBT data set, in the absence of synthesis with TOPEX altimetric sea level height data sets, has the ability to measure monthly grid point estimates of anomalous time rates of change of upper ocean heat storage to within approximately $\pm 10 \text{ W m}^{-2}$. The smaller relative accuracy in Figure 4 can be explained by considering spatial and temporal averaging over N independent estimates of grid point heat storage estimates. A value for N of 16 derives from two independent estimates in both zonal and meridional dimensions over the 10° latitude by 20° longitude boxes (i.e., with decorrelation space scales of 5° latitude and 20° longitude from *White* [1995]) and four independent estimates in yearly-time averages required to detect interannual variability (i.e., with decorrelation timescales of 3 months from *White* [1995]). Therefore, since standard errors of box-averages on interannual timescales decrease as the inverse of the square root of the number of independent estimates [Young, 1962], then grid point errors of $\pm 10 \text{ W m}^{-2}$ reduce to box averages errors of $2\text{-}3 \text{ W m}^{-2}$, as observed. Moreover, this level of accuracy seems to have been achieved in the flux-driven model by anomalous air-sea heat fluxes and horizontal heat transport divergences, suggesting that they have been estimated with grid point errors of $\pm 10 \text{ W m}^{-2}$.

6. Summary

Model ENSO timescale heat storage variations of the upper 400 m of the North Pacific Ocean showed good agreement when compared to heat storage observations.

The model results are also in general good agreement with previous descriptions of the anomalous circulation and thermal structure of the North Pacific Ocean. ENSO timescale heat storage and heat budget variability (3-4 year typical period) had maximum amplitudes in the $\pm 20^\circ$ equatorial band.

Heat storage variations consist of two parts, a diabatic contribution being forced by the surface heat flux Q (the temperature equation in our model) and an adiabatic contribution being controlled by inertial effects (the beta effect) and the wind stress curl. This latter contribution is the temperature-weighted model mass conservation equation. Adiabatic/diabatic ratios (the ratio of the last term to the second term in (2)) were computed for all six areas. The maximum ratios are achieved at those locations where it is believed that the Rossby wave activity is stronger. These waves propagate in the form of thermocline oscillations, and that is probably why we see the highest ratios along their path. Areas where these ratios are higher than, say, 2.2, have their total heat balance dominated by the time change of heat and the three-dimensional divergence of the heat flux.

With respect to the total heat budget the central NPO is dominated by the surface heat flux and the vertical heat transport through the 400-m level. At the western equatorial region, two separate balances seem to emerge: one is between the time change of heat and the horizontal divergence of the heat flux, and the other one is between the vertical heat transport and the surface heat flux that at this location has a damping role. A visual inspection of the spatial and temporal structure of the heat equation terms on several basin scale maps revealed that the dominant heat balance on a grid point (i.e., no spatial average) basis is between the time change of heat and the three-dimensional divergence of the heat flux for most locations.

On the other hand, the diabatic heat budget at mid-latitudes in the North Pacific is significantly influenced by meridional advection, so that a three-term approximate balance holds: local change, surface heat flux forcing, and meridional advection. The main conclusions about different heat budget components arising from this study are as follows:

In agreement with the analysis of SST tendency by *Barnett et al.* [1991] and *Battisti* [1988], the vertical advection term, at 400 m here, is of vital importance to close the total heat balance in the eastern equatorial Pacific. The presence of an eastern boundary forces arriving heat anomalies to either reflect, sink, and/or propagate poleward. It is still an open question how this heat is distributed once it sinks below the 400 m level and whether it has an important net contribution to the heat storage of the eastern equatorial ocean below 400 m. For ENSO timescales and along the equatorial strip the meridional advection term is of comparable amplitude to the zonal advection term on a regional average but of a bit smaller amplitude when compared

on a local (grid point-to-grid point) basis in the central and western parts. As a result of its coarse horizontal resolution, OPYC underestimates the amplitude of the meridional advection and the time change of heat terms at the eastern boundary of the Pacific Ocean. With the exception of areas 3 and 4 (central and Western subtropical), the four remaining selected areas show important and sometimes dominant contributions from horizontal advection to the total divergence of the horizontal heat flux. This is probably related to the fact that areas 3 and 4 have an intense isopycnal activity associated to the three-dimensional divergence of the mass flux.

In midlatitudes the net surface heat flux field has a key role in determining the field of the time change of heat storage in the upper 400 m of the North Pacific.

Only at the two equatorial areas analyzed here (western and eastern) does cross-isopycnal mixing have amplitudes comparable with those of vertical advection while at the remaining areas (extratropical), vertical advection dominates the total vertical heat transport (i.e., advection plus mixing).

It was shown in this study that different ENSO events are not always governed by the same physical processes, at least from the perspective given by the analysis of the heat budget in the upper 400 m of the North Pacific. The way in which heat is exchanged and transported in the North Pacific varies, in some cases, among different ENSO events. For instance, the model time series revealed that different ENSO events have different contributions from adiabatic and diabatic processes. Area 1 (western equatorial) has a dominant, or at least a very important, contribution to its heat budget from diabatic physics. Horizontal advection of heat plays a major role in this area. The opposite happens at the eastern equatorial region (area 2). For the 1972, 1976 and 1979 tropical warming events, diabatic processes dominated area 1, while adiabatic processes dominated area 2. Both contributions were comparable during the 1980s in both areas. Adiabatic processes dominated, on the other hand, the western subtropical Pacific (areas 3 and 4) during the 1970s and 1980s, areas where the Rossby wave activity is more intense and where contributions to the total budget from horizontal advection are negligible. The central north Pacific (area 5) was dominated by diabatic processes in the 1972 and 1986 ENSO episodes and diabatic and adiabatic processes were of comparable size in the 1976, 1979 and 1982 ENSOs. The California coastal region (area 6) was dominated by diabatic processes during the 1972 and 1976 ENSO events and by adiabatic fluxes during the 1982 and 1986 events. During these last two events meridional and vertical heat advection were dominant processes in the diabatic heat budget. The 1979 warming event was a transition with comparable contributions from both type of fluxes.

In summary, remarkable comparisons between model and observed heat storage have been presented in spite

of the coarse horizontal and vertical resolution of the ocean model. Given the spatial complexity of most of the heat equation terms observed at all locations in the North Pacific, we suggest that a more detailed analysis of the observations, this model hindcast and the output of coupled GCMs, be undertaken. This will more concretely verify what features are of ocean origin and what features are directly forced by the atmosphere. Obviously, there is much room for improving the model and obtaining more precise estimates of the large-scale processes found in this research. A necessary first step aimed to improve the performance of OPYC is the use of a much finer horizontal grid, which will be capable of resolving western boundary currents, coastally trapped waves and ultimately mesoscale variability. This use, combined with denser and better observations, especially surface heat fluxes in the tropics, will hopefully lead to smaller differences between model and observations and hence to a better understanding of the ocean interior dynamics and its interaction with the overlying atmospheric system.

Acknowledgments. Funding was provided by NOAA under the Scripps Experimental Climate Prediction Centre (NA67 GPO 450), the Lamont/Scripps Consortium for Climate Research (NA47 GPO 188), and the Paleoclimate Program (NA66 GPO 274). We are also supported by the National Space Development Agency of Japan (NASDA), under a joint program entitled 'Pacific Ocean Variations'.

References

- Alexander, M. A., Midlatitude atmosphere ocean interaction during El Niño: 1. The North Pacific Ocean, *J. Clim.*, 9, 944-958, 1977.
- Auad, G., A. J. Miller and, W. B. White, Simulation of heat storages and associated heat budgets in the Pacific Ocean. Part 2. Interdecadal timescale, this issue, 1998.
- Barnett, T.P., M. Latif, E. Kirk and, E. Roeckner, On ENSO Physics, *J. Clim.*, 4, 487-515, 1991.
- Battisti, D. S., Dynamics and thermodynamics of a warming event in a coupled tropical atmosphere-ocean model, *J. Atmos. Sci.*, 45, 2889-2919, 1988.
- Bryden H.L., D.H. Roemmich and, J. A. Church, Ocean heat transports across 24°N in the Pacific, *Deep-Sea Research*, 38, 297-324, 1991.
- Cayan D., A.J. Miller, T. P. Barnett, N. E. Graham, J. N. Ritchie and, J. M. Oberhuber, Seasonal-to-Interannual fluctuations in surface temperature over the Pacific: effects of monthly winds and heat fluxes, in *Natural Climate Variability on Decade-to-Century Time Scales*. National Research Council, edited by National Academy Press, Washington DC, 20418, pp. 133-150, 1995.
- Cayan, D. R., Latent and sensible heat flux anomalies over the northern oceans: Driving the sea surface temperature, *J. Phys. Oceanogr.*, 22, 859-881, 1992.
- Davis, R. E., Predictability of sea surface temperature and sea level pressure anomalies of the North Pacific, *J. Phys. Oceanogr.*, 6, 249-266, 1976.
- Deser, C., M. Alexander and, M. Timlin, Upper ocean thermal variations in the North Pacific during 1970-1991, *J. Clim.*, 8, 1840-1855, 1996.
- Jacobs, G.A., H.E. Hurlburt, J.C. Kindle, E.J. Metzger, J.L. Mitchell, W.J. Teague and, A.J. Wallcraft, Decade-scale

- trans-pacific propagation and warming effects of an El Niño anomaly, *Nature*, **370**, 360-363, 1994.
- Kaylor R. E., Filtering and decimation of digital time series, *Tech. Rep. BN 850*, 42 pp., Institute for Physical Science and Technology, University of Maryland, 1977.
- Killworth, P., Time interpolation of forcing fields in ocean models, *J. Phys. Oceanogr.*, **26**, 136-143, 1996.
- Latif, M. and, T. Barnett, Causes of decadal climate variability over the North Pacific and North America, *Science*, **266**, 634-637, 1994.
- Liu, Z., Thermocline forced by varying wind: Spin-up and spin-down, *J. Phys. Oceanogr.*, **23**, 2505-2522, 1993.
- Miller, A.J., D.R. Cayan, T. P. Barnett, N. E. Graham and, J. M. Oberhuber, The 1976-77 climate shift of the Pacific Ocean. *Oceanography*, **7**, 21-26, 1994a.
- Miller, A.J., D.R. Cayan, T. P. Barnett, N. E. Graham and, J. M. Oberhuber, Interdecadal Variability of the Pacific Ocean: model response to observed heat flux and wind stress anomalies, *Climate Dynamics*, **9**, 287-302, 1994b.
- Miller A. J., W. B. White and, D. R. Cayan, North Pacific Thermocline Variations on ENSO timescales, *J. Phys. Oceanogr.*, **27**, 2023-2039, 1997.
- Miller A. J., D. R. Cayan and, W. B. White, A decadal change in the North Pacific thermocline and gyre-scale circulation, *J. Clim.*, in press, 1998.
- Oberhuber J. M., Simulation of the Atlantic circulation with a coupled sea ice - mixed-layer isopycnal general circulation model. Part I: model description and part II: model experiment, *J. Phys. Oceanogr.*, **23**, 808-845, 1993.
- Robertson, A.W., Interdecadal variability over the North Pacific in a multi-century climate simulation, *Climate Dynamics*, **12**, 227-241, 1996.
- TOGA Numerical Experiment Group, *Comparison of TOGA Tropical Pacific Ocean Model Simulations with the WOCE/OGA Surface Velocity Programme Drifter Data Set*, 139 pp., Scripps Inst. of Oceanogr., La Jolla, Calif., 1995.
- White W. B., Design of a global observing system for gyre-scale upper ocean temperature variability, *Progress in Oceanography*, **36**, 169-217, 1995.
-
- G. Auad, A. Miller, and W. White, Climate Research Division, Scripps Institution of Oceanography, University of California, San Diego, 9500 Gilman Dr., La Jolla, CA 92093.
(e-mail: guillo@ucsd.edu)

(Received May 19, 1997; revised March 4, 1998;
accepted May 31, 1998.)